Viscous Shock-Layer Analysis of Two-Dimensional and Axisymmetric Flows

R. N. Gupta, E. V. Zoby, K.-P. Lee

Reprinted from

Journal of Thermophysics and Heat Transfer

Volume 8, Number 3, Pages 494–499

AIAA

A publication of the
American Institute of Aeronautics and Astronautics, Inc.
370 L'Enfant Promenade, SW
Washington, DC 20024-2518

JOURNAL OF THERMOPHYSICS AND HEAT TRANSFER
Vol. 8, No. 3, July–Sept. 1994

Viscous Shock-Layer Analysis of Two-Dimensional and Axisymmetric Flows

Roop N. Gupta* and Ernest V. Zoby*
NASA Langley Research Center, Hampton, Virginia 23681
and
Kam-Pui Lee†
ViGYAN, Inc., Hampton, Virginia 23666

Results are obtained for cylindrical leading edges of proposed transatmospheric vehicles by employing a two-dimensional viscous shock-layer code for nonequilibrium gas flows. The accuracy and efficiency of the planar code is verified through detailed comparisons with other predictions. This study includes results for 6-deg half-angle bodies with nose radii ranging from 0.01 to 2.0 ft for both cylindrically blunted wedges and spherically blunted cones (included for comparison). Some results are presented as a ratio of the noncatalytic to the corresponding fully catalytic heating value to illustrate the maximum potential for a heating reduction in dissociated nonequilibrium flows. Generally, this ratio and the individual heating rates are smaller for cylindrically blunted wedges with small nose radii as compared to the spherically blunted cones (for the same nose radius). Therefore, a larger potential exists for heating reduction in cylindrically blunted as compared with the spherically blunted surfaces. However, the results presented at higher altitudes (where the slip effects become important) show that the spherically blunted nose gives lower stagnation-point heating due to stronger merged shock-layer effects as compared with a cylindrically blunted nose.

Nomenclature

a_c, b_c, c_c, d_c, e_c = coefficients appearing in Eq. (5)
C_f = skin-friction coefficient, $2\tau_w^*/(\rho_\infty^* U_\infty^{*2})$
C_H = heat transfer coefficient, $2q^*/(\rho_\infty^* U_\infty^{*3})$
$C_{p,\infty}^*$ = freestream specific heat
g = stretching function
h_1 = $1 + n_{sh}\bar{\eta}\kappa$
h_3 = $r + \bar{\eta} n_{sh} \cos\theta$
M_∞ = freestream Mach number
$\bar{M}^*$ = molecular weight of mixture
n = coordinate measured normal to the body, n^*/R_N^*
p = pressure, $p^*/(\rho_\infty^* U_\infty^{*2})$
q = heat-transfer rate, $q^*/(\rho_\infty^* U_\infty^{*3})$
R_N^* = nose radius
r = radius of the body surface r^*/R_N^*
s = distance measured along the body surface, s^*/R_N^*
T = temperature, T^*/T_{ref}^*
T_{ref}^* = $U_\infty^{*2}/C_{p,\infty}^*$
U_∞^* = freestream velocity
u = velocity component tangent to body surface, u^*/U_∞^*
v = velocity component normal to body surface, v^*/U_∞^*
x = axial body coordinate
α = shock angle defined in Fig. 1
β = angle defined in Fig. 1
γ_i = recombination coefficient for species i
$\Delta\eta$ = stepsize in η direction
$\Delta\xi$ = stepsize in ξ direction
η = transformed $\bar{\eta}$ coordinate, $g(\bar{\eta})$
$\bar{\eta}$ = transformed n coordinate, n/n_{sh}
θ_b = body angle defined in Fig. 1
κ = body curvature, $\kappa^* R_N^*$
ξ = coordinate measured along the body
ρ = density of mixture, ρ^*/ρ_∞^*
τ^* = shear stress

Subscripts
BL = boundary layer
c = cylinder
FCW = fully catalytic wall
m = grid-point location along the body
NCW = noncatalytic wall
n = grid-point location normal to the body
PG = perfect gas
ref = reference
s = sphere
sh = shock
VSL = viscous shock layer
w = wall
∞ = freestream

Superscripts
$*$ = dimensional quantity
$-$ = quantity divided by corresponding shock value
$'$ = total differentiation with respect to ξ

Presented as Paper 93-2751 at the AIAA 28th Thermophysics Conference, Orlando, FL, July 6–9, 1993; received July 15, 1993; revision received Dec. 17, 1993; accepted for publication Dec. 18, 1993.

*Senior Research Engineer, Aerothermodynamics Branch, Space Systems Division. Associate Fellow AIAA.
†Research Engineer. Senior Member AIAA.

Introduction

HIGH-PERFORMANCE transatmospheric vehicles,[1] which fly at hypersonic speeds for both ascent and entry conditions, are characterized by small radius leading edges. These geometries, while aerodynamically desirable, result in large convective heating rates. The leading edges, in particular for the wings, must maintain a known surface geometry and should not experience a recession of the surface. Conse-

quently, the leading edges will have to be actively cooled to ensure that these surfaces remain at an acceptable temperature. Since these surfaces can constitute many linear feet, the required weight of coolant would be substantial. This increased coolant weight, unfortunately, may translate to a reduction in deliverable payload weight. Therefore, it is important to accurately predict the surface heating at the leading edges.

The aerothermal environment about these small leading edges is dominated by viscous nonequilibrium effects. The investigation of Ref. 2 demonstrated the conservatism involved in heating calculations based on equilibrium rather than a nonequilibrium assumption. The calculations were performed for a range of nose radii and freestream conditions. These calculations, however, were restricted to axisymmetric leading edges only. Presently proposed vehicles have leading edges ranging in shapes from three-dimensional to two-dimensional (cylindrical).

The initial purpose of the present investigation was to obtain nonequilibrium viscous shock-layer results for the two-dimensional flows and compare them with the corresponding axisymmetric calculations.[3,4] While this work does not allow a direct assessment of a proposed leading edge, the modified code does give the vehicle designer a qualitative assessment of surface heating and subsequent cooling requirements for the nonaxisymmetric leading edges.

This study documents a parametric comparison of nonequilibrium surface heating levels for sphere-cone (axisymmetric) and cylinder-wedge (two-dimensional) shaped 6-deg half-angle bodies for different nose radii using the viscous shock-layer (VSL) equations. The results are presented primarily for relatively large Reynolds number conditions, but some are also shown (for a sphere and a cylinder) from a Navier-Stokes solution procedure[5] with surface slip at low Reynolds number conditions. These results provide a comparison between the planar and axisymmetric stagnation-point heating under low-density conditions. Emphasis is placed on smaller nose radii bodies and lower altitudes.

Analysis

Governing Equations

The conservation equations employed in the present analysis are the steady VSL equations for nonequilibrium flow over a two-dimensional body at 0-deg angle of attack (see Fig. 1). The normalized form of these equations in the orthogonal, body-oriented, transformed coordinates may be obtained from Refs. 4, 6, and 7 by setting the variable "j" to zero. The major difference between the two-dimensional flow and axisymmetric flow ($j = 1$) lies in the form of the global continuity equation, which for a two-dimensional flow is

$$\frac{\partial}{\partial \xi}\left[n_{sh}\rho_{sh}u_{sh}\bar{\rho}\bar{u}\right] + \frac{dg}{d\bar{\eta}}\frac{\partial}{\partial \eta}\left[h_1\rho_{sh}\bar{\rho}v - n'_{sh}\bar{\eta}\rho_{sh}u_{sh}\bar{\rho}\bar{u}\right] = 0 \quad (1)$$

where

$$h_1 = 1 + n_{sh}\bar{\eta}\kappa \quad (2)$$

Boundary Conditions and Flowfield Properties

Most of the results presented here are with the no slip boundary condition at shock and body. The shock boundary condition for no slip case is obtained from the Rankine-Hugoniot relations. The shock and surface slip boundary conditions (implemented for low density flows) are obtained from Refs. 7 and 8, respectively.

For nonequilibrium airflow, a seven-species (N_2, O_2, N, O, NO, NO^+, and e$^-$) chemical model is used to evaluate the species production terms that appear in the energy and species continuity equations. The expressions and the reaction rates used to compute the production terms in the present study

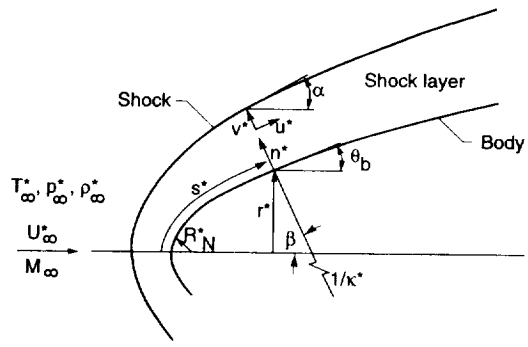

Fig. 1 Coordinate system.

are taken from Ref. 9 and are similar to those of Ref. 10. Details for the computation of production terms are provided in Ref. 4.

The thermodynamic properties for specific heat and enthalpy, and transport properties for viscosity and thermal conductivity are obtained by using curve fits of Ref. 9. The semi-empirical method of Wilke[9] is used to calculate the gas-mixture viscosity. The Prandtl number is set equal to 0.72, whereas the Lewis number is assigned a value of 1.4 with an assumption of binary diffusion.

Method of Solution

The numerical method used for solving the two-dimensional VSL equations is the same as that employed for axisymmetric bodies.[3,4,11] However, the shock standoff distance n_{sh} at a specified body station m is obtained from the integration of Eq. (1)

$$(n_{sh})_m = \left\{\left[n_{sh}\rho_{sh}u_{sh}\int_0^1\left(\bar{\rho}\bar{u}\Big/\frac{dg}{d\bar{\eta}}\right)d\eta\right]_{m-1} - \Delta\xi_{m-1}\left[h_1\rho_{sh}v_{sh} - n'_{sh}\rho_{sh}u_{sh} - \rho_{sh}v_{sh}(\mathrm{FLUXW})\right]_{m-1/2}\right\}\Big/\left[\rho_{sh}u_{sh}\int_0^1\left(\bar{\rho}\bar{u}\Big/\frac{dg}{d\bar{\eta}}\right)d\eta\right]_m \quad (3)$$

where

$$\mathrm{FLUXW} = (\bar{\rho}\bar{v})_w \quad (4)$$

which is zero in the absence of injection through the surface.

Equation (3) is different than that for an axisymmetric flow, where a quadratic equation for n_{sh} is obtained.[4]

The first-order global continuity equation [Eq. (1)] is rewritten (at a given body station m) as

$$(a_c)_{n+1/2}v_{m,n+1} + (b_c)_{n+1/2}v_{m,n} + (c_c)_{n+1/2}\bar{\rho}_{m,n+1} + (d_c)_{n+1/2}\bar{\rho}_{m,n} = (e_c)_{n+1/2} \quad (5)$$

with the help of the equation of state

$$\bar{\rho} = (\bar{p}/\bar{T})(\bar{M}^*/\bar{M}^*_{sh}) \quad (6)$$

which is employed to eliminate the density $\bar{\rho}$ from Eq. (1). Equation (5) is similar in form to that given in Ref. 4 for an axisymmetric flow and is solved in a similar coupled way with the normal momentum equation. The coefficients appearing in Eq. (5), however, are different from those given in Ref. 4 and are provided in Appendix A of Ref. 12. The coefficients for the n-momentum equation are the same as those given in Ref. 4.

A procedure similar to that of Ref. 4 is also used to obtain the stagnation-point solution. This solution is obtained by

expanding the various flowfield quantities in terms of distance ξ along the body surface. These expansions reduce the partial differential equations to ordinary differential equations at the stagnation-point singularity ($\xi = 0$) which may be integrated normal to the surface with appropriate shock and surface boundary conditions. The solution procedure[3,4] then marches along the body using the stagnation-point solution.

The Vigneron condition[3] is used for the pressure gradient in the streamwise momentum equation in the subsonic nose region. The global iterations are employed in this region to update the pressure (and shock shape). In the supersonic flow region, the pressure gradient term is approximated with a two-point backward difference, and a predictor-corrector approach[3] is used for the shock shape to march the solution downstream. It should be mentioned that unlike the axisymmetric calculations,[3,6] converged results cannot be obtained for the two-dimensional shape without the use of Vigneron condition.

Results and Discussion

Detailed results from nonequilibrium calculations are presented in this section. First, a comparison with existing numerical predictions is provided. Results for a cylindrically blunted slender wedge and a spherically blunted cone for a range of nose radii are presented next. Some results are also provided as a ratio of the noncatalytic heating to the corresponding fully catalytic value. This ratio (which is also a measure of the degree of flowfield nonequilibrium) demonstrates the maximum potential for a surface heating-rate reduction in the presence of dissociated nonequilibrium flow. Finally, some results from the planar and axisymmetric flow calculations are also included at higher altitudes using the stagnation region Navier-Stokes code of Ref. 5 with surface slip. Reference 12 contains comparisons and other detailed calculations for the perfect-gas flows.

Comparison with Other Predictions

Present predictions are compared with those obtained from LAURA[13,14] in Figs. 2a and 2b for a fully catalytic wall. Both the calculations give similar qualitative results. The maximum difference between the surface pressure predictions (Fig. 2a) is about 10%, whereas for the surface heat transfer rate (Fig. 2b) it is about 20%. These differences are believed to be due to the different transport and thermodynamic properties employed in the two predictions. Presently, it is being planned to implement the properties from Ref. 9 (employed in the present calculations) in code LAURA.

Comparison with Axisymmetric Calculations and Parametric Studies

Two-Dimensional and Axisymmetric Calculations

Results from a comparative study of the cylindrically blunted wedge and spherically blunted cone are shown in Fig. 3. These calculations are for 6-deg half-angle noncatalytic bodies with a nose radius of 0.125 ft along a surface distance of 300 nose radii. The shock inflection shown in Fig. 3a for the sphere-cone calculations is not noticeable for the cylinder-wedge predictions. The effect of this shock inflection is seen in the surface pressure distribution of Fig. 3b and heating rate distribution of Fig. 3c. For cylinder-wedge calculations, the surface quantities continuously decrease beyond the tangency point. In the stagnation region and its immediate vicinity, the surface pressures are almost same for the two calculations as shown in Fig. 3b. However, due to the larger shock standoff distance for the cylindrically blunted wedge as compared to a sphere cone (Fig. 3a), the surface heating-rate values are generally lower than those predicted for a spherically blunted cone. There is a slight crossover (not noticeable in Fig. 3c)

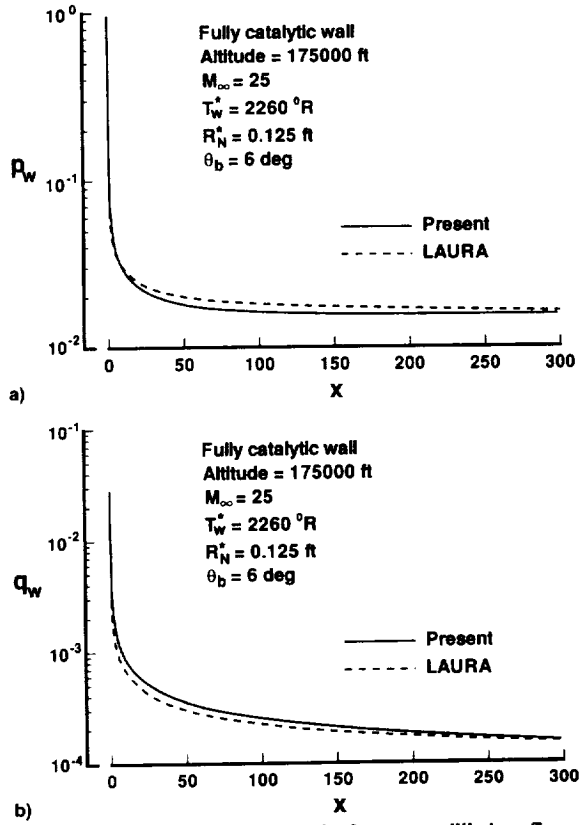

Fig. 2 Comparison of predicted results for nonequilibrium flow over a 6-deg cylindrically blunted wedge: a) surface pressure distribution and b) surface heat transfer rate distribution.

of the predicted distributions due to overexpansion and recompression of the flow over a spherically blunted cone.

Bluntness Effects

Similar to the studies of Refs. 2 and 15, nose bluntness effects are studied through the ratio of noncatalytic to fully catalytic heating rates. This ratio shows the maximum potential for a heating reduction in dissociated nonequilibrium flow, with a smaller value of the ratio implying a larger potential for reduction. For a finite catalytic wall this ratio will be larger and, therefore, the actual heating reduction would be less than the values shown in Fig. 4. This figure gives the heating reduction ratio through a wetted distance of 30 ft for nose radii values of 0.125 and 0.25 ft. The heating-reduction ratio generally decreases to a value of less than 0.40 over the spherical (or cylindrical) nose portions of the body. This ratio stays less than this value for a cylinder-wedge for running lengths of less than 30 ft. The ratio becomes as large as 0.9 for a sphere-cone body.

It may be noticed from Fig. 4 that the heating ratio for a sphere cone rapidly approaches a value of about 0.9 on the downstream side for the smaller ($R_N^* = 0.125$ ft) nose radius. For such large values of the ratio, a finite-catalytic wall boundary condition would have a very small influence on the heating. A large value of the heating ratio for a low angle sphere-cone is due to the fact that the effects of dissociated species, which are produced primarily in the stagnation region, diminish on the surface heating as the flow spreads over a larger surface area at these conditions.

For the two nose radii considered in Fig. 4, the heating-rate distributions for a fully catalytic wall are given in Fig. 5. This figure when used with Fig. 4 can give the individual heating reduction for a given nose radius. The heating rate values for a cylinder-wedge, in general, are lower than the sphere-cone values (by as much as 50% for $R_N^* = 0.125$ ft and $s^* = 30$ ft). For the larger nose radius ($R_N^* = 0.25$ ft),

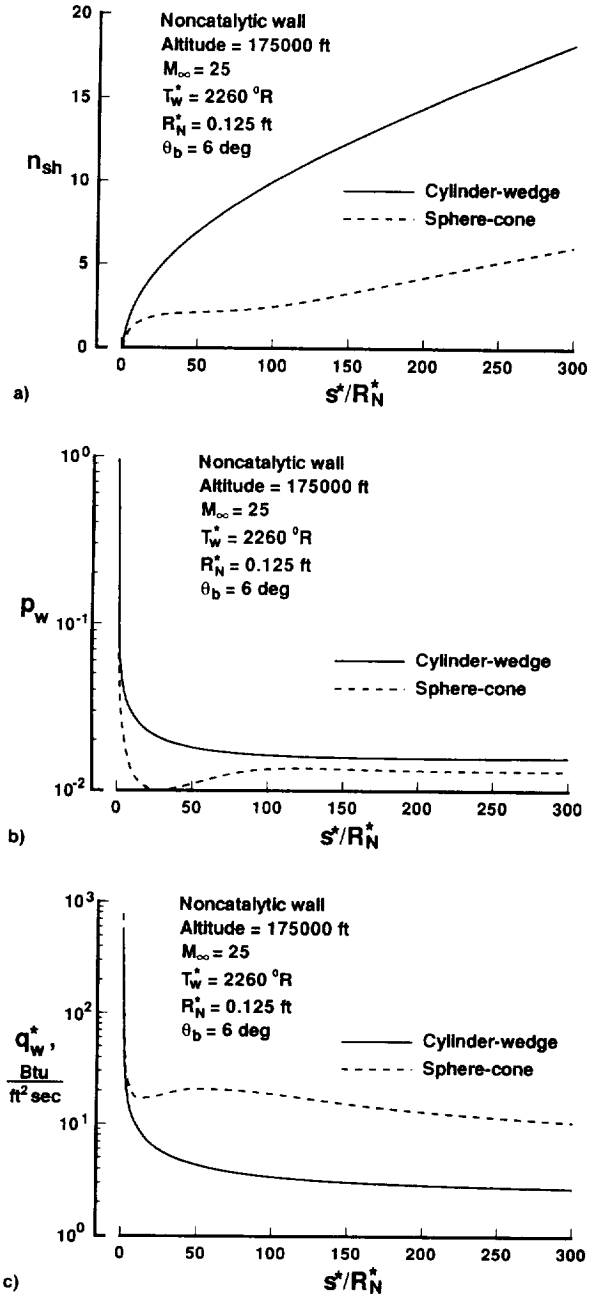

Fig. 3 Comparison of shock standoff distance and surface quantities for 6-deg two-dimensional (cylinder-wedge) and axisymmetric (sphere-cone) bodies in nonequilibrium flow: a) shock standoff distance, b) pressure distribution, and c) heat transfer rate distribution.

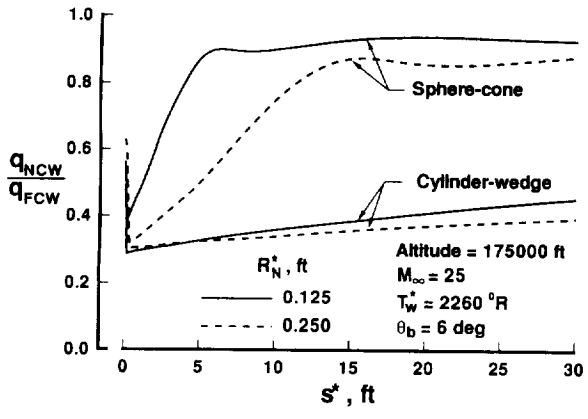

Fig. 4 Nonequilibrium heating ratio vs wetted distance.

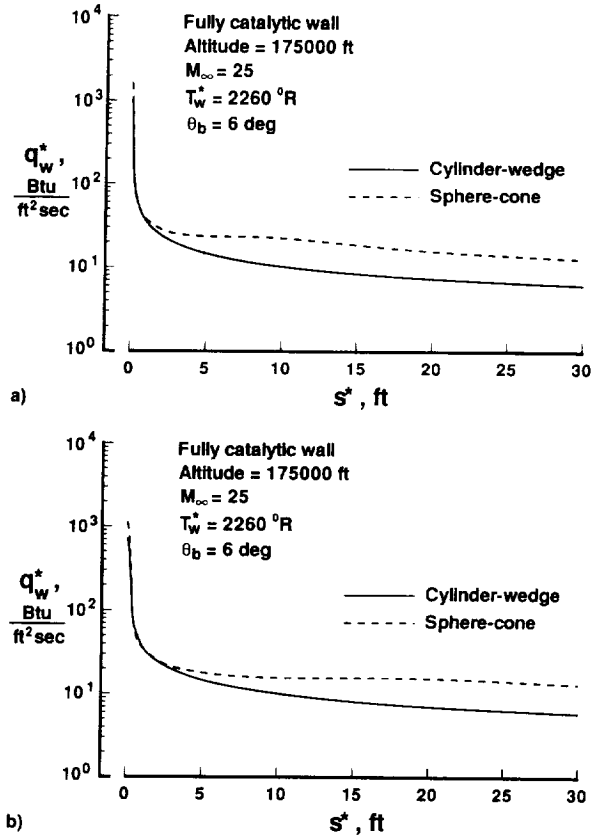

Fig. 5 Nonequilibrium heat-transfer rate distribution for different nose radii: a) $R_N^* = 0.125$ ft and b) $R_N^* = 0.25$ ft.

differences between the two predictions decrease. Reference 12 also provides results for $R_N^* = 0.5$ and 1.0 ft.

Stagnation-Point Heating vs Nose Radius

The heating-reduction ratio as a function of nose radius is shown in Fig. 6a. The heating ratios for both cylinder and sphere calculations first decrease to minimum values (maximum nonequilibrium conditions), and then increase with the increase in nose radius. This trend with increasing radius is due to the flowfield chemistry changing from frozen state to equilibrium condition. A lower value of the heating ratio implies a higher degree of nonequilibrium. For flows with a low heating-ratio value, considerable reduction in fully catalytic wall heating value can be obtained by making the surface noncatalytic. Figure 6a shows that the flowfield chemistry "freezes" slower with the decrease in nose radius for a cylinder (due to large relaxation distance) as compared with a sphere. Therefore, a bigger potential exists for the surface heating reduction for smaller nose radii cylindrically blunted bodies.

The heating-reduction ratio of Fig. 6a shows a potential for reduction. It does not, however, give actual values for the heating reduction. These values are given in Fig. 6b. Figure 6a gives the same two-dimensional value of about 0.5 for heating reduction for nose radii of about 0.01 and 0.06 ft. However, the actual noncatalytic wall (NCW) heating value in Fig. 6b at $R_N^* = 0.01$ ft is about 3 times the value at $R_N^* = 0.06$ ft. Similarly, the same axisymmetric heating-reduction ratio of 0.5 for $R_N^* = 0.04$ and 0.15 ft (from Fig. 6a) gives actual values which differ by a factor of 1.5 (Fig. 6b). Thus, Fig. 6b gives the required heating values to a designer. However, the fully catalytic wall values of Fig. 6b can be reduced by making the surface noncatalytic as shown in this figure. The percentage of reduction for a given nose radii can be obtained from Fig. 6a.

Figure 6c compares the stagnation point heating on a spherical nose for a range of nose radii. The present VSL heating rates obtained for equilibrium flow chemistry are almost sim-

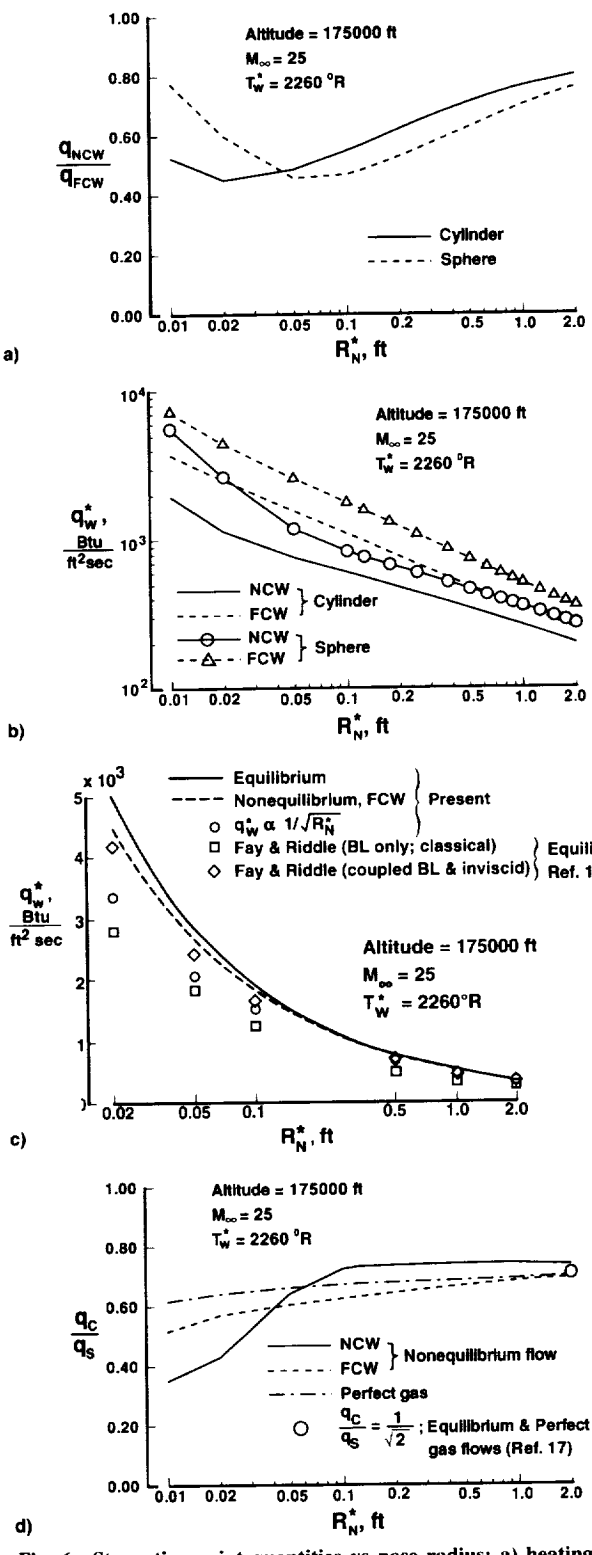

Fig. 6 Stagnation-point quantities vs nose radius: a) heating ratio, b) heating rates, c) heating rates (for sphere), and d) heating ratio.

ilar to those predicted for nonequilibrium flow chemistry with the fully catalytic wall boundary condition, except for the smaller ($R_N^* < 0.2$ ft) nose radii. Clearly, the present heating results do not scale as $1/\sqrt{R_N^*}$ for smaller values of the nose radii due to large viscous and nonequilibrium effects. The classical boundary-layer result of Fay and Riddell[15,16] is also shown along with the coupled boundary layer and inviscid calculations[17] for equilibrium flow chemistry. The coupled calculations give results which are within 4 and 17% of the equilibrium VSL results at nose radii of 2.0 and 0.02 ft, respectively. These calculations are obviously in better agreement with the VSL predictions than the classical boundary-layer results of Fay and Riddell. Since the results for the two-dimensional (cylindrical stagnation point) calculations scale as $1/\sqrt{2}$ with the corresponding axisymmetric (spherical nose) computations for equilibrium flow chemistry,[18] differences in the various heating rates for the two-dimensional computations are expected to be similar to those shown in Fig. 6c.

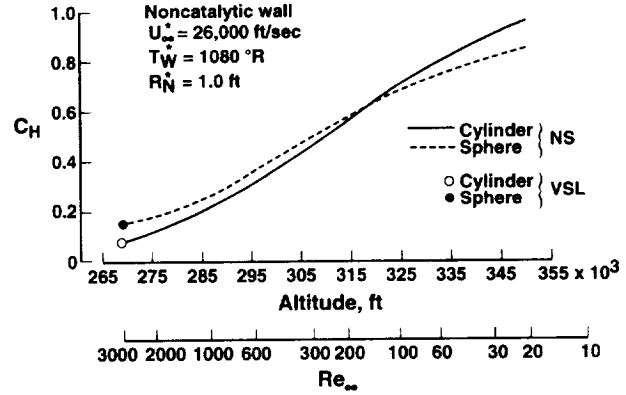

Fig. 7 Comparison of stagnation-point heat transfer coefficient for a cylinder and a sphere with slip.

Present calculations for nonequilibrium flow chemistry with noncatalytic and fully catalytic walls are intended to provide lower and upper bounds, respectively, for the heating rates to a designer. Therefore, no results are presented as a function of the recombination rate parameter as provided in Ref. 16. In addition, since a corresponding approximate nonequilibrium analysis (for use with the Fay and Riddell's correlation for frozen flow) is not available, a comparison of Fay and Riddell's results with the VSL nonequilibrium calculations is not provided.

The stagnation-point heating for a cylinder is, generally, lower than that for a sphere as shown in Fig. 6d. For a noncatalytic surface, the heating rate for a cylinder q_c is 35% of the sphere value q, at $R_N^* = 0.01$ ft, and increases to about 75% at $R_N^* = 0.5$ ft before decreasing slightly. For a fully catalytic wall, the cylinder value increases from about 50 to 70% of the sphere value over the range of nose radius shown in Fig. 6d. The cylinder values range between 60–70% of the sphere values for the perfect gas calculations[12] shown here. Also given in this figure is a value of $1/\sqrt{2}$ for the equilibrium and perfect-gas flows.[18] For larger nose radius, nonequilibrium values of the q_c/q ratio appear to approach this value.

Stagnation-Point Results at Higher Altitudes

The viscous shock-layer results presented so far are for lower altitude flight conditions and have been obtained without the slip conditions. Some stagnation-point surface heat transfer results have also been obtained at higher altitudes, where the slip conditions become important. The present viscous shock-layer method with surface[8] and shock slip[7] is employed at an altitude of 270,000 ft, and a Navier-Stokes solution procedure[5] with surface slip[8] is used for altitudes equal to and greater than 270,000 ft. The two methods give almost similar values for the heat transfer coefficients for both a cylinder and a sphere at the common altitude of 270,000 ft as shown in Fig. 7. One interesting point to note in this figure is that stagnation-point heat transfer coefficient for a sphere becomes smaller than the corresponding value for a cylinder for altitudes greater than about 315,000 ft. This is a consequence of the stronger merged shock-layer effect on a sphere as compared with a cylinder.

Concluding Remarks

Results are presented from the study of two-dimensional nonequilibrium VSL flows. These are among the earliest VSL results for such flows reported in the literature. Comparisons

of the present results are made with those obtained from the Navier-Stokes LAURA algorithm, and the results compare well. These comparisons indicate that the present planar code is as accurate and requires as few computer resources as its axisymmetric counterpart when compared to LAURA. The axisymmetric flow results are included in the present study to highlight the differences between the planar and axisymmetric flows.

The investigation includes a detailed study of the nose bluntness effects on the stagnation point as well as downstream nonequilibrium flow conditions. The downstream influence of nonequilibrium flow for a small nose radius two-dimensional body is found to be much smaller than for the larger nose radii. Although a ratio of noncatalytic to fully catalytic heating rates was used to characterize the maximum potential for a nonequilibrium heating reduction over the range of conditions, a comparison of individual stagnation heating rates demonstrated that a comparison of the same ratio value was not indicative of the actual heating reduction. Furthermore, the fully catalytic wall heating rates (which are closer to the equilibrium value) illustrate the amount of conservatism contained in such a calculation, as compared with a noncatalytic (or finite-catalytic) wall value. This conservatism would result in excessive coolant requirement at the cost of deliverable payload.

Generally, the heating-rate values for a cylindrically blunted wedge are lower than those for a spherically blunted cone, except at very high altitudes. Under those low-density conditions the merged shock-layer effects seem to be stronger for a sphere than for a cylinder. This results in lower heating for a spherical than for a cylindrical stagnation point.

Acknowledgments

The authors would like to thank P. A. Gnoffo and C. J. Riley for obtaining the LAURA results included here.

References

[1]Williams, R. M., "National Aero-Space Plane: Technology for America's Future," *Aerospace America*, Vol. 24, No. 11, 1986, pp. 18–22.

[2]Zoby, E. V., Lee, K. P., and Gupta, R. N., "Hypersonic Nonequilibrium Viscous Solutions over Slender Bodies," *Journal of Spacecraft and Rockets*, Vol. 28, No. 3, 1991, pp. 358–360.

[3]Gupta, R. N., Lee, K. P., Zoby, E. V., Moss, J. N., and Thompson, R. A., "Hypersonic Viscous Shock-Layer Solutions over Long Slender Bodies—Part I: High Reynolds Number Flows," *Journal of Spacecraft and Rockets*, Vol. 27, No. 2, 1990, pp. 175–184.

[4]Lee, K. P., and Gupta, R. N., "Viscous-Shock-Layer Analysis of Hypersonic Flows over Long Slender Vehicles," NASA CR-189614, March 1992.

[5]Gupta, R. N., and Simmonds, A. L., "Hypersonic Low-Density Solutions of the Navier-Stokes Equations with Chemical Nonequilibrium and Multicomponent Surface Slip," AIAA Paper 86-1349, June 1986.

[6]Moss, J. N., "Reacting Viscous-Shock Layer Solutions with Multicomponent Diffusion and Mass Injection," NASA TR-411, June 1974.

[7]Gupta, R. N., Nayani, S. N., Lee, K. P., and Zoby, E. V., "Higher-Order Viscous Shock-Layer Solutions for High Altitude Flows," AIAA Paper 93-2724, July 1993.

[8]Gupta, R. N., Scott, C. D., and Moss, J. N., "Slip-Boundary Equations for Multicomponent Nonequilibrium Air Flows," Appendix D, NASA TP-2452, Nov. 1985; also *Thermal Design of Aeroassisted Orbital Transfer Vehicles*, edited by H. F. Nelson, Vol. 96, Progress in Astronautics and Aeronautics, AIAA, New York, 1985, pp. 465–490.

[9]Gupta, R. N., Yos, J. M., Thompson, R. A., and Lee, K. P., "A Review of Reaction Rates and Thermodynamic and Transport Properties for an 11-Species Air Model for Chemical and Thermal Nonequilibrium Calculations to 30000 K," NASA RP-1232, Aug. 1990.

[10]Blottner, F. G., "Viscous Shock Layer at the Stagnation Point with Nonequilibrium Air Chemistry," *AIAA Journal*, Vol. 7, No. 12, 1969, pp. 2281–2288.

[11]Gupta, R. N., Lee, K. P., and Zoby, E. V., "Enhancements to Viscous-Shock-Layer Technique," *Journal of Spacecraft and Rockets*, Vol. 30, No. 4, 1993, pp. 404–413.

[12]Gupta, R. N., Lee, K. P., and Zoby, E. V., "A Viscous Shock-Layer Analysis of 2-D and Axisymmetric Flows," AIAA Paper 93-2751, July 1993.

[13]Gnoffo, P. A., "Hypersonic Nonequilibrium Flow over a Cylindrically Blunted 6° Wedge," NASA TM-108994, Aug. 1993.

[14]Gnoffo, P. A., Gupta, R. N., and Shinn, J. L., "Conservation Equations and Physical Models for Hypersonic Air Flows in Thermal and Chemical Nonequilibrium," NASA TP-2867, Feb. 1989.

[15]Zoby, E. V., Lee, K. P., Gupta, R. N., Thompson, R. A., and Simmonds, A. L., "Viscous Shock-Layer Solutions with Nonequilibrium Chemistry for Hypersonic Flows Past Slender Bodies," *Journal of Spacecraft and Rockets*, Vol. 26, No. 4, 1989, pp. 221–228.

[16]Fay, J. A., and Riddell, F. R., "Theory of Stagnation Point Heat Transfer in Dissociated Air," *Journal of Aeronautical Sciences*, Vol. 25, No. 2, 1958, pp. 73–85.

[17]Zoby, E. V., and Simmonds, A. L., "Engineering Flowfield Method with Angle-of-Attack Applications," *Journal of Spacecraft and Rockets*, Vol. 22, No. 4, 1985, pp. 398–404.

[18]Anderson, J. D., Jr., "Hypersonic and High Temperature Gas Dynamics," McGraw-Hill, New York, 1989.